Expanding Differential Ion Mobility Separations into the MegaDalton Range

Tobias P. Wörner,[1] Hayden A. Thurman,[2] Alexander A. Makarov,[1,3] Alexandre A. Shvartsburg[2,*]

1. Thermo Fisher Scientific, Hanna-Kunath Strasse 11, Bremen 28199, Germany
2. Department of Chemistry, Wichita State University, 1845 Fairmount, Wichita, KS 67260
3. Biomolecular Mass Spectrometry and Proteomics, Bijvoet Centre for Biomolecular Research and Utrecht Institute for Pharmaceutical Sciences, Utrecht University, Padualaan 8, 3584 CH Utrecht, The Netherlands

* e-mail: alexandre.shvartsburg@wichita.edu

ABSTRACT: Along with mass spectrometry (MS), ion mobility separations (IMS) are advancing to ever larger biomolecules. The emergence of electrospray ionization (ESI) and native MS had enabled the IMS/MS analyses of proteins up to ~100 kDa in 1990s and whole protein complexes and viruses up to ~10 MDa since 2000s. Differential IMS (FAIMS) is substantially orthogonal to linear IMS based on absolute mobility K and offers exceptional resolution, unique selectivity, and steady filtering readily compatible with slower analytical methods such as the electron capture or transfer dissociation (ECD/ETD). However, the associated MS stages had limited FAIMS to ions with m/z < 8,000 and masses under ~300 kDa. Here we integrate high-definition FAIMS with the Q-Exactive Orbitrap UHMR mass spectrometer that can handle m/z up to 80,000 and MDa-size ions in the native ESI regime. In the initial evaluation, the oligomers of monoclonal antibody adalimumab (148 kDa) are size-selected up to at least the nonamers (1.34 MDa) with m/z up to ~17,000. This demonstrates the survival and efficient separations of non-covalent MDa assemblies in the FAIMS process, opening the door to novel analyses of heaviest macromolecules.

Mass spectrometry (MS) has tackled ever larger targets, expanding from atomic ions to organic molecules, amino acids, lipids and peptides, proteins and their assemblies, and viruses.[1-5] This evolution was enabled by novel ion sources allowing soft ionization of increasingly large biomolecules, especially ESI with no size limit and multiple charging that kept the ion mass/charge (m/z) ratio in a tight low range over multiple orders of magnitude[6,7] of m. Most analyses utilized substantially acidic and/or organic ESI solvents for highest ion signal and z values to minimize m/z. Native ESI/MS methods maximally retain the solution conformations of fragile biomolecules, including the non-covalent complexes critical to protein function, by employing the solvents that mimic the physiological conditions and minimizing the ion excitation during the ESI desolvation and in downstream MS stages.[8,9]

Complex samples require fractionation before the MS step.[10] The traditional liquid chromatography and electrophoresis techniques are progressively replaced or complemented by ion mobility spectrometry (IMS) in gases that offers speed and unique selectivity.[11-14] Linear IMS approaches[11,12] rely on the absolute K values at a typically moderate electric field (E). The differential or field asymmetric waveform IMS (FAIMS) exploits the $K(E)$ dependence to separate and identify the ion moieties by ΔK - the increment of K between two E levels.[11,13,14]

An asymmetric waveform of some amplitude (dispersion voltage, U_D) establishes an oscillatory field across the gap of width g between two parallel electrodes.[14] This field (with the peak strength $E_D = U_D/g$) deflects the ions pushed through the gap by gas flow toward either electrode at an angle set by ΔK at the E levels in two waveform polarities. A compensation field ($E_C = U_C/g$) of compensation voltage (U_C) superimposed on the waveform can offset this motion for a given species to pass, while others still drift toward the electrodes and are destroyed on impact. Scanning U_C elicits the spectrum of ions entering the gap. The resolving power (R) maximizes in the gaps with homogeneous field between planar electrodes,[14,15] scaling as $t^{1/2}$ where t is the separation time inversely proportional to the volume gas flow rate (Q). Further maximizing R by employing wider gaps that allow longer t, smoothed waveforms, maximum U_D near electrical breakdown, and buffers comprising He or H_2 produces "high-definition FAIMS".[16,17] The devices with inhomogeneous field between curved electrodes augment sensitivity at lower R via ion focusing to the gap median.[14,15,18,19]

Strong correlation between the ion mass and physical size constrains linear IMS in conjunction with MS.[20] The mass or m/z correlate to ΔK much weaker[21] than to K, making MS more orthogonal to FAIMS than linear IMS- by (3 - 6)× for typical biomolecules.[22-24] Hence, FAIMS resolves most isomers better than the linear IMS with same R metric - in particular for lipids,[22] peptides with sequence inversions or alternative post-translational modification (PTM) sites,[23] and diastereomers.[24] For instance,[24] the D/L peptides are resolved better by FAIMS with mean R ~ 90 than linear IMS with R ~ 180. Same holds for the isotopomers[25] and structurally specific E_C shifts between the isotopologues of small molecules.[26,27] However, linear IMS can elucidate the molecular conformations by comparing the measured collision cross sections (Ω) with those computed for trial geometries.[28,29] The much more difficult calculations of high-field K remain too crude for same capability with FAIMS.

As most IMS implementations have no inherent mass limit, the m and m/z ranges of ESI/IMS/MS platforms were defined by the ESI and MS stages and followed them up with time. The advances in native MS expanded linear IMS from single-strand proteins[28] to larger complexes such as the ferritin 24-mer (480 kDa), GroEl (800 kDa) and viruses/capsids up to ~10 MDa.[29,31-33] Those studies have furnished valuable insights into the subunit connectivity and morphology of such objects.

The species analyzed by FAIMS were much smaller. The histone tails (5.5 kDa) with variant PTM sites[34] and conformers and protomers for proteins up to ~80 kDa co-eluting in linear IMS[35-41] were resolved. In top-down proteomics, FAIMS separations raise the sequence coverage and the number of detected proteins and proteoforms up to 30 kDa.[2,43] The combinations of FAIMS with H/D exchange or ECD have probed the protein folding in more detail.[35,36] The protein aggregates were separated up to 147 kDa (tetramer of alcohol dehydrogenaze, ADH)[44] under the native ESI conditions and 332 kDa (pentamer of bovine serum albumin, BSA)[45] upon denaturation..

Ions in linear IMS normally rotate freely and the orientationally-averaged Ω_{Avg} determine the K values.[11] Much stronger fields in differential IMS can lock[38,39] the permanent dipoles into pendular states with the mobility controlled by the directional Ω in plane perpendicular to the dipole ($\Omega_{\perp}$). That requires[39] the dipole moment (p) to exceed a threshold depending on $\Omega_{\perp}$ and the gas pressure (P) and temperature (T), in theory ~400 Debye (D) for the typical protein ions generated by denaturing ESI at $P \sim 1$ Atm and $T \sim 300$ K. As statistically the dipoles point roughly along the principal molecular axis, generally $\Omega_{\perp} < \Omega_{Avg}$ and the alignment should lift the K values manifesting in $E_C < 0$ (versus $E_C > 0$ for rotary macroions).[38,39] The dipole moment - the (separated charges) × (their distance) - broadly increases for heavier proteins with larger z and size,[39] and the trend line crosses 400 D at ~30 kDa. Indeed, the denatured proteins above ~30 kDa such as carbonic anhydrase (29 kDa), ADH (37 kDa), and BSA (66 kDa) show intense signal at $E_C < 0$ whereas smaller ones [e.g., ubiquitin (8.6 kDa), cytochrome c (12 kDa), and myoglobin (17 kDa)] do not.[35-41,45,46]

Material FAIMS effects for rotary species typically require $E > 15$ kV/cm (at $P = 1$ Atm), but much weaker fields can lock strong dipoles.[45] In the low-field differential (LOD) IMS governed solely by the dipole alignment, all rotary species come at $E_C = 0$ while the values for aligned macroions scale linearly with E_D (versus E_D^3 in FAIMS)[45,46] and the E_D intercept and slope of $E_C(E_D)$ function provide the information on p and $\Omega_{\perp}/\Omega_{Avg}$ quantities. The p values for ADH and BSA monomers and oligomers with various numbers of units (n) ranged up to 6 kD in line with the solution measurements and molecular modeling, expectedly increasing from ADH to larger BSA and for greater n and z values.[45,46] The native proteins and complexes exhibited no signal at $E_C < 0$ (indicating alignment) up to the maximum studied $m = 147$ kDa,[44] or ~5× the threshold to lock the denatured conformers. With native ESI, the m/z of ions markedly increases for heavier proteins. Hence, the analyses of larger native species were hampered by the m/z limits of MS platforms previously available with FAIMS: 8,000 for Orbitrap Eclipse[44] and 4,000 for other Orbitrap or ion trap instruments.[34,38-40]

The most biomedically consequential large proteins are antibodies (Ab) central to immunology.[47] These Y-shaped glycoproteins (~150 kDa) contain two heavy and two light chains tied by disulfide (S-S) bridges. Of the five Ab classes (IgA, IgD, IgE, IgG, IgM), the IgG is most studied and prevalent in therapeutics. The IgG1 (Adalimumab, 148.4 kDa) - a recombinant human monoclonal Ab (mAb) specific to the tumor necrosis factor - was approved in 2002 as Humira™ to treat arthritis, psoriasis, and ulcerative colitis, paving the way to ~100 current mAb drugs.[48] Immunoglobulins routinely form oligomers with $n \leq 6$ critical to the biological function.[49-53] In native MS, their overlapping charge state envelopes pose a real analytical challenge.[48,49,54] Size-exclusion chromatography partly resolved the species with $n = 1$, 2, and {3; 4}, but not 3 from 4 or any $n > 4$ from those or each other.[49,53,55] Much smaller peptide/protein oligomers (in terms of total and monomer masses, commonly amyloid or D-amino acid containing peptides) with same m/z were size-selected by linear IMS[56-60] and FAIMS.[45,64] Previously FAIMS was applied to the light and heavy mAb chains (23 and 51 kDa),[61] but not the intact Abs.

Here we extend the m/z range of FAIMS by 10× via coupling it to the Thermo Scientific Q-Exactive Orbitrap UHMR™ mass spectrometer with $m/z = 80{,}000$ limit[9] and analyzing the intact antibodies and complexes into the MDa range.

Experimental Methods

The ambient-pressure planar-gap FAIMS stage ($g = 1.88$ mm)[17,34,45,46] was attached to the MS inlet capillary by a custom holder with ~2.5 mm air gap (Figure S1). An ESI emitter was placed in front of the FAIMS curtain plate (CP)/orifice aperture in one electrode. A bisinusoidal waveform with 2:1 harmonic ratio and 1 MHz frequency at U_D up to 4.6 kV (i.e., E_D up to 24.5 kV/cm) was applied to the opposite electrode. The U_C scan at the 0.5 V/min speed was superimposed on the waveform. The dc biases (to ground) were 5 kV on the emitter, 1 kV on the CP, and ~20 V on the FAIMS cell and MS inlet. The UHP N_2 carrier gas was supplied by a digital flowmeter at $Q = 4$ L/min producing $t \sim 75$ ms.[62] Exceeding our "standard" $Q = 2$ L/min (for $t \sim 150$ ms) reduces the FAIMS resolution but maximizes the ion flux (scaling as e^{-t}).[15,63] That is important for large macromolecules and especially complexes because of the necessarily low solution molarity and ion signal spread over many oligomer states and z values, and often wide E_C ranges for each.[45,46]

Suitably for large species, the Orbitrap ion transfer target and detector were at "high m/z". We set the capillary temperature to 330 °C and S-lens rf level to 150. The in-source-trapping, injection flatapole, inter flatapole, bent flatapole, and transfer multipole were at −150, 5, 4, 2, and 0 V, respectively. Spectra were recorded at the resolution setting of 1,563 with 10 microscans and 100 ms injection time. The N_2 collision gas setting was 4 (UHV pressure of 1.5 E−10 mbar).

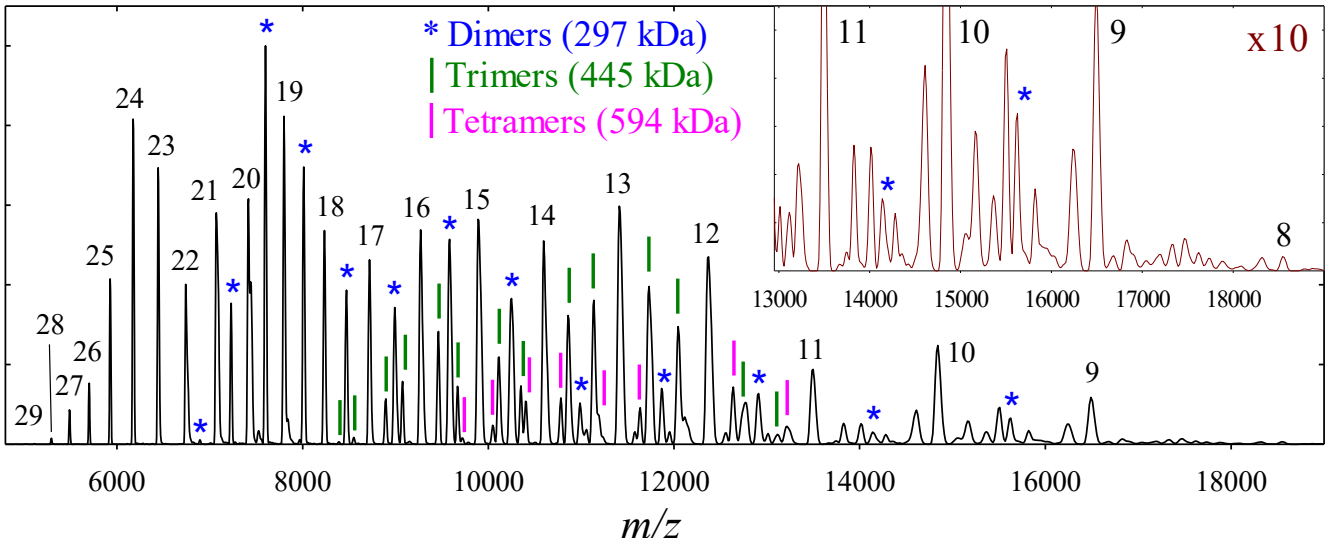

Figure 1. The mass spectrum of IgG1 sample, with the charge states for nominal monomers and color-coded labels for the nominal dimers, trimers, and tetramers. The upper *m*/*z* segment is enlarged in the inset.

The over-the-counter Humira preparation (AbbVie) aged by five years was buffer-exchanged into the 0.2 M NH_4Ac solution[64] and diluted to ~10 uM in the H_2O/CH_3CN solvents with 50 - 100% H_2O. The sample was infused to the ESI source at 1 uL/min by a syringe pump.

Results and Discussion

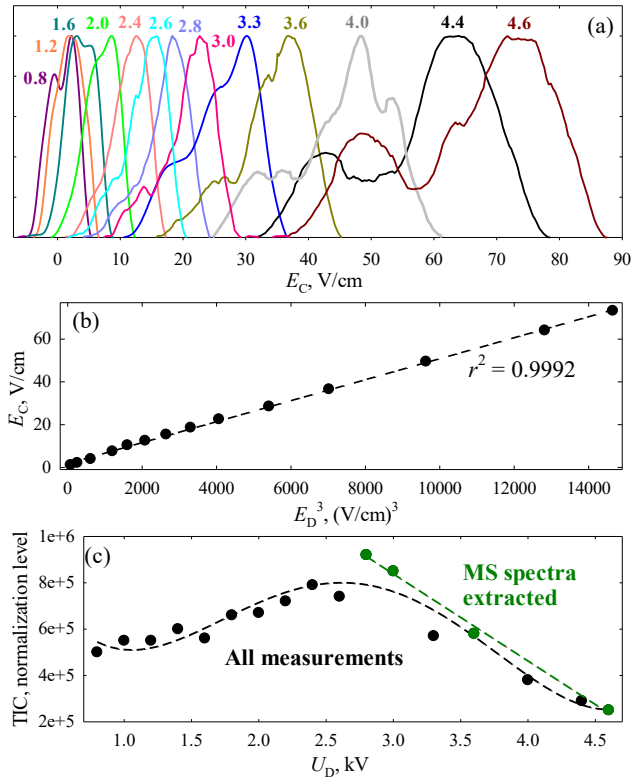

Figure 2. (a) Normalized TIC FAIMS spectra as a function of U_D as labeled; (b) ion signal depending on U_D, highlighting the values selected for data analysis (dashed lines are regressions through the data); (c) the $E_C(E_D^3)$ trend for major peaks: measurements (circles) and linear regression (line).

The MS envelope at 50% H_2O (Figure S2a) contains mostly IgG1 monomers (z = 17 - 61) plus small amounts of dimers (z_2 = 33 - 91) and trimers (z_3 = 55 - 109), in line with our findings for BSA and ADH.[45,46] At 60% and 90% H_2O, the maximum z decreases to ~40 and ~30, respectively, with similar drops for z_2 and z_3. The peaks for dimers and especially larger oligomers grow to match those for monomers in some *m*/*z* ranges (Figure S2 b, c). Removing the last 10% CH_3CN hardly affects the spectrum (Figure S2d), but harms the ion signal and ESI stability.

Hence, we picked the 90:10 H_2O/CH_3CN solvent for all FAIMS analyses. The mass spectrum occupies the *m*/*z* ~5,000 - 19,000 range, consisting of the peaks for monomers (z = 8 - 29), dimers (z_2 = 19 - 43), trimers (z_3 = 34 - 53), tetramers (z_4 = 45 - 61), and larger non-deciphered oligomers at *m*/*z* >13,000 (Figure 1). As the peak heights for nominal monomers with z = 18 - 20 are interpolations of those for adjacent dimers with odd z_2, those are essentially dimers too. The "monomers" with $z \le 17$ rising above the neighboring dimers must be due to the addition of trimers emerging at that point and then all oligomers. Then the "dimers" with $z_2 \le 27$ are similar in intensity to adjacent tetramers and are mostly tetramers.

The total ion count (TIC) FAIMS scans are near-Gaussian at E_C = 0 up to U_D = 1 kV, meaning no separation (Figure 2a). At higher U_D up to the maximum, they progressively move in the positive E_C direction while broadening and splitting off one or two significant features on the low-E_C side. No peaks at E_C < 0 suggest no alignment. The $E_C(E_D)$ curve for major peaks is near-perfectly cubic (Figure 2b), confirming the true FAIMS (not LODIMS) separation mechanism.[14,45,46]

The peak TIC increases some from U_D = 0 to 2.8 kV, then drops ~4× up to the maximum 4.6 kV (Figure 2c). Such signal increase up to some U_D point is not surprising and perhaps ensues from the field heating in the gap improving ion desolvation. The decrease at higher U_D is usual, reflecting faster ion losses with accelerated anisotropic diffusion and greater ion oscillation amplitude in the waveform cycle,[14,15] fragmentation or isomerization of fragile species in the gap upon stronger heating,[45] and spread of signal over the expanding E_C space.

The overall trends of mass spectra across FAIMS scans are the same at U_D = 3.0 kV with best signal, the maximum U_D = 4.6 kV, and intermediate 3.6 kV (Figures S3 - S5). The *m*/*z*

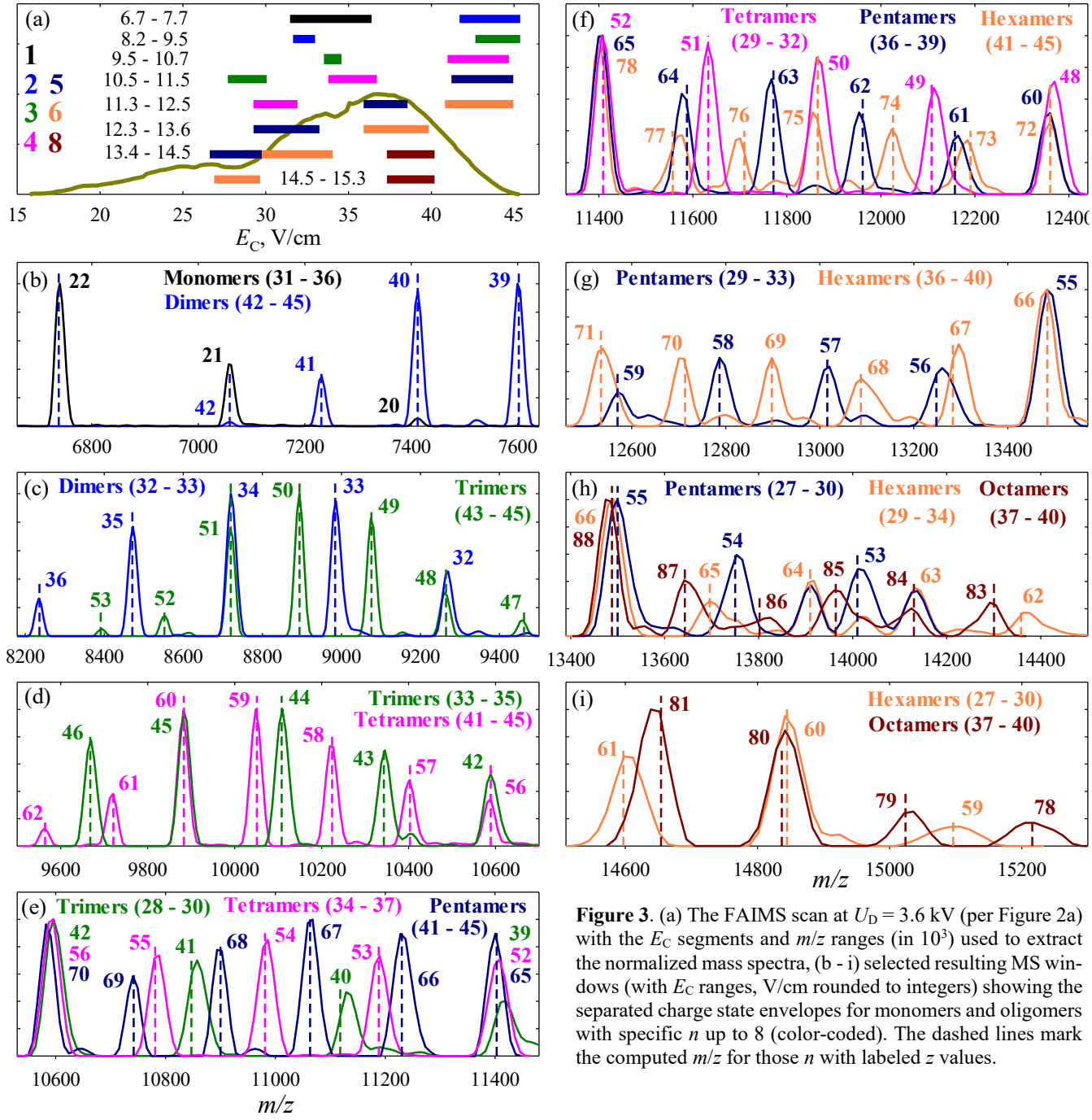

Figure 3. (a) The FAIMS scan at U_D = 3.6 kV (per Figure 2a) with the E_C segments and m/z ranges (in 10^3) used to extract the normalized mass spectra, (b - i) selected resulting MS windows (with E_C ranges, V/cm rounded to integers) showing the separated charge state envelopes for monomers and oligomers with specific n up to 8 (color-coded). The dashed lines mark the computed m/z for those n with labeled z values.

ranges move up with decreasing E_C values, as known for the compact proteins across the charge states. The oligomer size separations are evident in the relevant MS spectral windows. While the monomers and dimers largely lie apart in terms of m/z, the minor overlaps in the ~7,000 - 7,400 range ($z = 20/z_2 = 40$ and $z = 21/z_2 = 42$) are disentangled at $U_D \geq 3$ kV, Figure 3. Different oligomers overlap more in MS (as anticipated from the closer relative n), but all up to $n = 6$ are cleanly resolved by FAIMS. While the optimum U_D depends on the n values and m/z ranges, U_D = 3.6 kV provides excellent separations up to n = 8 (Figure 3 c - h).

Examples include the baseline resolution of dimers (297 kDa) and trimers (445 kDa) overlapping at m/z ~ 8,300 - 9,500 (specifically the $z_2 = 32/z_3 = 48$ and $z_2 = 34/z_3 = 51$ isobars) in Figure 3c and trimers and tetramers (594 kDa) at m/z ~ 9,500 - 11,400 (z_3 of 39, 42, 45 versus z_4 of 52, 56, 60, respectively) in Figure 3 d, e. We further separate the larger oligomers mixed in original mass spectra: pentamers (742 kDa) from trimers and tetramers at m/z ~ 10,600 - 11,400 (in the $z_3 = 39/z_4 = 52/z_5 = 65$ and $z_3 = 42/z_4 = 56/z_5 = 70$ triplets) in Figure 3e and hexamers (890 kDa) from tetramers and pentamers at m/z ~ 11,400 - 12,400 ($z_4 = 48/z_5 = 60/z_6 = 72$ and $z_4 = 52/z_5 = 65/z_6 = 78$) in Figure 3f. Here, the m/z distributions for successive n get close enough to merge across three n, but all are resolved by FAIMS. The pentamers and hexamers are similarly separated over higher m/z ~12,500 - 13,500 with the resolved $z_5 = 55/z_6 = 66$ pair, but no heptamers were encountered (Figure 3g). Finally, the hexamers and octamers (1.19 MDa) are separated in the m/z ~ 13,400 - 15,200 range with the disentangled $z_6 = 60/z_8 = 80$ and $z_6 = 66/z_8 = 88$ pairs (Figure 3h, i).

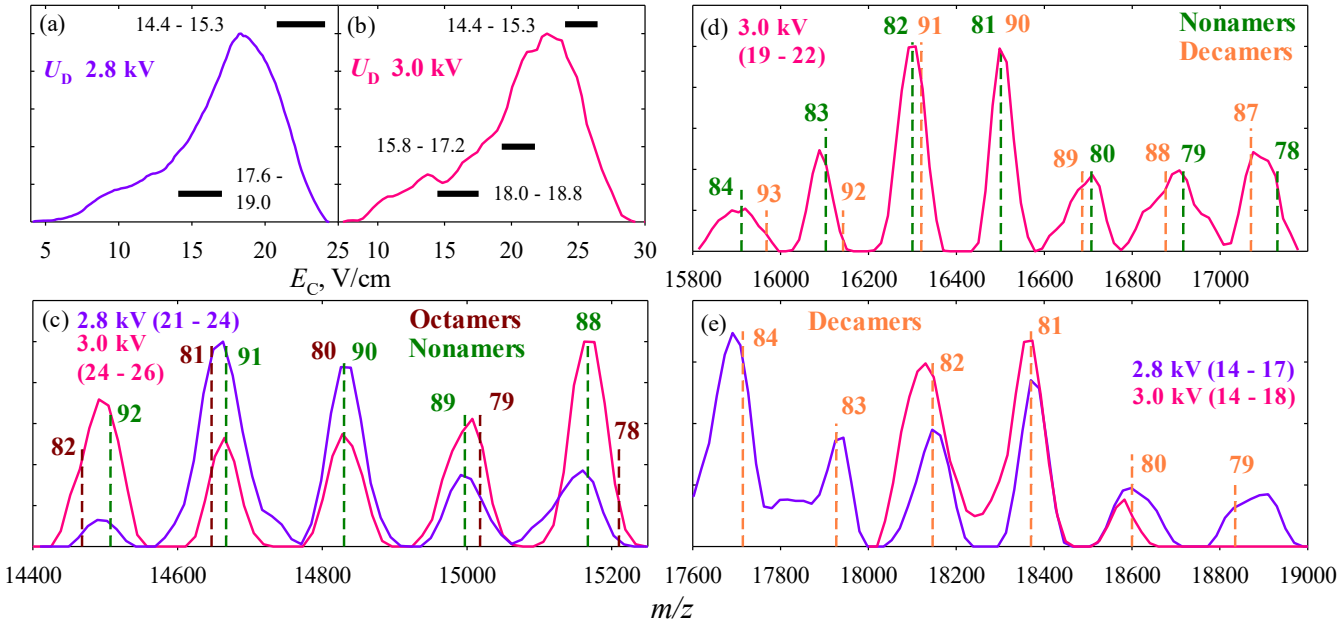

Figure 4. (a, b) Normalized FAIMS scans at U_D of 2.8 and 3.0 kV (per Figure 2a) with the E_C segments and m/z ranges (in 10^3) used to extract the normalized mass spectra as labeled, (c - e) selected MS windows at those U_D values (color-coded) and E_C ranges (V/cm rounded to integers given). The dashed lines mark the computed m/z for specific n (color-coded) with labeled z values.

The distributions for $n \leq 6$ resemble those for IgG under native ESI conditions[50,54] with the m/z ranges of ~5,500 - 7,000 (n = 1), ~7,000 - 9,000 (n = 2), ~9,000 - 11,000 (n = 3), ~10,000 - 12,500 (n = 4), and ~12,000 - 15,000 (n = 6): the presence of 10% CH_3CN had little effect in accord with Fig. S2. The previously unreported octamers come at m/z = 13,400 - 15,200, following the above progression. This trend mirrors our findings for the ADH and BSA species:[45,46] presumably the attenuated Coulomb repulsion with lower charge density at greater m/z stabilizes the larger oligomers with weaker bonding.

The E_C values rapidly increase upon charging for all n with near-uniform slopes (Figure 3a). This trend tracks that for small proteins (e.g., ubiquitin or cytochrome c) over a low-z range with compact conformers, but not over the full z range involving an abrupt E_C drop upon unfolding.[36,38,40,65] This indicates present species staying compact at all z, appropriately for the mAbs held by the S-S bonds and the native ESI regime.

The accurate m/z for nominal isobars inch up at lower n values. This suggests an incomplete desolvation with more solvent molecules per subunit in smaller oligomers (e.g., ensuing from their larger surface area per subunit). However, this mass shift varies and is insufficient to distinguish any overlaps.

The above trends are reproduced at U_D = 4.6 kV (Figure S6), but the size separation is not visibly enhanced. That may reflect the noisier spectra at lower ion counts (especially for larger oligomers disproportionately fragmented by field heating) and/or the conformational ensembles (created by said heating) interfering with the size discrimination.

While the spectra at $U_D \geq 3.6$ kV are blank at $m/z \geq 15{,}000$, the MS-only spectrum shows substantial signal up to m/z ~ 18,000 - 19,000 (Figure 1). That reveals the species fragmented by field heating in the FAIMS cell.[45,65] As the increment of ion temperature over gas temperature (ΔT) scales approximately as E_D^2 and thus U_D^2 per the two-temperature theory,[11,65,66] the larger (generally more fragile) oligomers survive better at lower U_D values.[45] Same was observed for the peptide oligomers in traveling-wave IMS with also substantial field heating.[56]

Here we see consistent MS peaks with m/z ~ 15,000 - 18,000 at U_D = 2.2 - 3.0 kV, where ΔT is ~40 - 70% of that at U_D = 3.6 kV and ~20 - 40% of that at 4.6 kV. As the E_C and therefore R values diminish at lower U_D (Figure 2), the ion preservation and separation are best balanced at 2.8 - 3.0 kV with also maximum total signal (Figure 4). With less peak separation for successive n because of lower R (~50 - 60% that at U_D = 3.6 kV assuming the cubic E_D scaling) and closer relative n values for larger n, multiple oligomer compositions may co-elute.

At top E_C values, the scans with U_D of 2.8 and 3.0 kV yield MS envelopes over m/z ~ 14,400 - 15,300 corresponding to the nonamers (1.34 MDa) with potential octamer impurity for the two lower-m/z peaks (Figure 4c). At E_C below the apex of scan at U_D = 3.0 kV, we see further nonamers at m/z ~ 15,700 - 17,200 with decamers (1.48 MDa) possibly present for the higher-m/z peaks (Figure 4d). At yet lower E_C in both scans, the peaks over the highest m/z ~ 17,600 - 19,000 range reasonably fit the decamers (Figure 4e). In summary, the nonamers come at m/z ~14,500 - 17,000 (properly above the range for n = 8) and decamers at yet higher m/z ~16,600 - 19,000.

Traces of even larger oligomers appear near the FAIMS scan apex at U_D of 2.8 and 3.0 kV (Figure S7). The peaks over m/z ~ 16,400 - 17,200 range at U_D = 2.8 kV cluster closer than the decamers and about right for the dodecamers (1.78 MDa), Figure S7c. In a slightly lower E_C range, the scans at both U_D exhibit a peak pattern over m/z ~ 17,000 - 18,000 best matching the 15-mers (2.23 MDa), Figure S7d. The exact compositions remain speculative and probably comprise a mixture.

The FAIMS data allow confident annotation of spectrum in Figure 1 up to m/z ~ 13,500 with the actual $n \leq 6$ and their superpositions (Figure S8). The smaller features at higher m/z could not be assigned for the noise/congestion, illustrating why larger oligomers were not heretofore reported.

Conclusions

We have enabled the differential IMS (FAIMS) capability on the Q-Exactive Orbitrap UHMR mass spectrometer. As the

effective FAIMS mass range is capped by the detector, this expands separations to the m/z = 80,000 limit of this MS instrument - an order of magnitude above the prior maximum[44] of m/z = 8,000. Incorporating the high-definition FAIMS stage and Orbitrap MS also delivers the high resolution in both dimensions crucial for modern biological analyses.[34]

The new system was initially assessed in the analyses of intact monoclonal antibodies, namely adalimumab (148 kDa), under near-native ESI source conditions. The mass spectra extended to $m/z \sim 19{,}000$, including numerous oligomers up to the tetramers and larger assemblies not identifiable because of the spectral congestion. All FAIMS scans at any dispersion field (E_D) up to the maximum 25 kV/cm resided in the positive compensation field (E_C) range, with pertinent E_C values scaling as E_D^3 throughout the E_D range. This behavior is a hallmark of classic FAIMS based on the field-dependent evolution of ion temperature rather than the electric dipole alignment ubiquitous for the denatured large proteins and complexes.[14]

The oligomers up to n = 8 (m = 1.2 MDa) with $m/z \leq 15{,}000$ were completely size-separated by FAIMS at U_D = 3.6 kV and identified by the MS charge state envelopes. The smaller peaks at higher m/z were found only at $U_D \leq 3$ kV, presumably because of dissociation upon heating in stronger fields. These were attributed to larger oligomers with n = 9 (1.3 MDa) and, tentatively because of weak signal and poor FAIMS resolution at lower U_D levels, $n \sim 10$ - 15 ($m \sim 1.5$ - 2.2 MDa). These species go beyond the already discovered mAbs oligomers ($n \leq 6$) and may be physical aggregates from solution (feasibly tied to the sample age) and/or ESI process with marginal or no biological role. That would most clearly illustrate the FAIMS separations of weakly bound complexes into the MDa range.

The E_C values for any given n continuously increase at higher z, indicating the conserved compact geometries. That and low charge density (seen in high m/z values) apparently engender the dipole moments p under ~400 D, precluding the pendular alignment as explained above. This is in agreement with the investigations[44] for "native" protein complexes up to ~150 kDa. The still larger (>2 MDa) and/or less rigid native species might accumulate sufficient p values to align in FAIMS.

Present mAbs oligomers exceed the heaviest species heretofore resolved by differential IMS[45] by over fourfold in m/z and mass itself. The m/z ceiling of new platform lies another 4× above the range covered in this work, permitting analyses of yet much larger macromolecules.

As FAIMS has no intrinsic mass limit and present stage was used as is, other FAIMS systems could likewise be coupled to UHMR MS. However, the optimum FAIMS mechanical and operational parameters (gap width, waveform frequency, and filtering time) hinge on the mobilities (K) and diffusion constants (D) of target ions.[14,67] Hence, the stages redesigned for much lower K and D values of MDa species ought to perform better.

Supporting Information

Photos of the instrument, mass spectra with different solvents and across the FAIMS scans at three U_D values, selected MS windows at U_D = 2.8, 3.0, and 4.6 kV.

ACKNOWLEDGMENT

This research was supported by the NSF CAREER (CHE-1552640) and RPG (CHE-2105182) grants. We thank Gordon A. Anderson (GAACE) for experimental assistance.

REFERENCES

1. Gross, J. H. *Mass Spectrometry: A Textbook*; Springer, **2017**.
2. Biemann, K. *Angew. Chem*. **1962**, *1*, 98.
3. Cajka, T.; Fiehn, O. *TrAC* **2014**, *61*, 192.
4. Wysocki, V. H.; Resing, K. A.; Zhang, Q.; Cheng, G. *Methods* **2005**, *35*, 211.
5. Wörner, T. P.; Shamorkina, T. M.; Snijder, J.; Heck, A. J. R. *Anal. Chem*. **2021**, *93*, 620.
6. Wong, S. F.; Meng, S. K.; Fenn, J. B. *J. Phys. Chem.* **1988**, *92*, 546.
7. Loo, J. A. *Mass Spectrom. Rev*. **1997**, *16*, 1.
8. Robinson, C. V. *Proc. Natl Acad. Sci. USA* **2019**, *116*, 2814.
9. Tamara, S.; den Boer, M. A.; Heck, A. J. R. *Chem. Rev*. **2022**, *122*, 7269.
10. Covey, T. R; Lee, E. D.; Bruins, A. P.; Henion, J. D. *Anal. Chem*. **1986**, *58*, 1451 A.
11. Mason, E. A.; McDaniel, E. W. *Transport Properties of Ions in Gases*; Wiley: New York, **1988**.
12. Eiceman, G. A., Karpas, Z., Hill, H. H. *Ion Mobility Spectrometry*; CRC Press: Boca Raton, FL, **2013**.
13. Guevremont, R. *J. Chromatogr. A* **2004**, *1058*, 3.
14. Shvartsburg, A. A.; Tang, K.; Smith, R. D. *J. Am. Soc Mass Spectrom.* **2004**, *15*, 1487.
15. Shvartsburg, A. A. *Differential Ion Mobility Spectrometry*; CRC Press: Boca Raton, FL, **2008**.
16. Shvartsburg, A. A.; Smith, R. D *J. Am. Soc. Mass Spectrom*. **2007**, *18*, 1672.
17. Shvartsburg, A. A.; Seim, T. A.; Danielson, W. F.; Norheim, R.; Moore, R. J.; Anderson, G. A.; Smith, R. D. *J. Am. Soc. Mass Spectrom.* **2013**, *24*, 109.
18. Guevremont, R.; Purves, R. W. *Rev. Sci. Instrum.* **1999**, *70*, 1370.
19. Swearingen, K. E.; Moritz, R. L. *Expert Rev. Proteomics* **2012**, *9*, 505.
20. Fenn, L. S.; Kliman, M.; Mahsut, A.; Zhao, S. R.; McLean, J. A. *Anal. Bioanal. Chem*. **2009**, *394*, 235.
21. Shvartsburg, A. A.; Mashkevich, S. V.; Smith, R. D. *J. Phys. Chem. A* **2006**, *110*, 2663.
22. Shvartsburg, A. A.; Isaac, G.; Leveque, N.; Smith, R. D.; Metz, T. O. *J. Am. Soc. Mass Spectrom.* **2011**, *22*, 1146.
23. Shvartsburg, A. A.; Creese, A. J.; Smith, R. D.; Cooper, H. J. *Anal. Chem.* **2011**, *83*, 6918.
24. Berthias, F.; Baird, M. A.; Shvartsburg, A. A. *Anal. Chem.* **2021**, *93*, 4015.
25. Kaszycki, J. L.; Bowman, A. P.; Shvartsburg, A. A. *J. Am. Soc. Mass Spectrom*. **2016**, *27*, 795.
26. Williamson, D. L.; Nagy, G. *Anal. Chem*. **2022**, *94*, 12890.
27. Pathak, P.; Baird, M. A.; Shvartsburg, A. A. *Anal. Chem.* **2018**, *90*, 9410.
28. Ho, K. M.; Shvartsburg, A. A.; Pan, B.; Lu, Z. Y.; Wang, C. Z.; Wacker, J. G.; Fye, J. L.; Jarrold, M. F. *Nature* **1998**, *392*, 582.
29. Ruotolo, B. T.; Benesch, J. L. P.; Sandercock, A. M.; Huyng, S. J.; Robinson, C. V. *Nat. Protoc*. **2008**, *3*, 1139.
30. Jarrold, M. F. *Acc. Chem. Res*. **1999**, *32*, 360.
31. Kaddis, C. S.; Lomeli, S. H.; Yin, S.; Berhane, B.; Apostol, M. I.; Kickhoefer, V. A.; Rome, L. H.; Loo, J. A. *J. Am. Soc. Mass Spectrom*. **2007**, *18*, 1206.
32. Uetrecht, C.; Rose, R. J.; van Duijn, E.; Lorenzen, K.; Heck, A. J. R. *Chem. Soc. Rev.* **2010**, *39*, 1633.
33. Knapman, T. W.; Morton, V. L.; Stonehouse, N. J.; Stockley, P. G.; Ashcroft, A. E. *Rapid Commun. Mass Spectrom*. **2010**, *24*, 3033.
34. Baird, M. A.; Shliaha, P. V.; Anderson, G. A.; Moskovets, E.; Laiko, V.; Makarov, A. A.; Jensen, O. N.; Shvartsburg, A. A. *Anal. Chem.* **2019**, *91*, 6918.
35. Purves, R. W.; Barnett, D. A.; Ells, B.; Guevremont, R.

J. Am. Soc. Mass Spectrom. **2001**, *12*, 894.
36. Robinson, E. W.; Williams, E. R. *J. Am. Soc. Mass Spectrom.* **2005**, *16*, 1427.
37. Robinson, E. W.; Leib, R. D.; Williams, E. R. *J. Am. Mass Spectrom*. **2006**, *17*, 1470.
38. Shvartsburg, A. A.; Bryskiewicz, T.; Purves, R. W.; Tang, K.; Guevremont, R. *J. Phys. Chem. B* **2006**, *110*, 21966.
39. Shvartsburg, A. A.; Noskov, S. Y.; Purves, R. W.; Smith, R. D. *Proc. Natl Acad, Sci USA* **2009**, *106*, 6495.
40. Shvartsburg, A. A. *Anal. Chem.* **2014**, *86*, 10608.
41. Zhang, J. D.; Donor, M. T.; Rolland, A. D.; Leeming, M. G.; Wang, H.; Trevitt, A. J.; Kabir, K. M. M.; Prell, J. S.; Donald, W. A. *Int. J. Mass Spectrom.* **2020**, *457*, 116425.
42. Fulcher, J. M.; Makaju, A.; Moore, R. J.; Zhou, M.; Bennett, D. A.; De Jager, P. L.; Qian, W. J.; Pasa-Tolic, L.; Petyuk, V. A. *J. Proteome Res*. **2021**, *20*, 2780.
43. Gerbasi, V. R.; Melani, R. D.; Abbatiello, S. E.; Belford, M. W.; Huguet, R.; McGee, J. P.; Dayhoff, D.; Thomas, P. M.; Kelleher, N. L. *Anal. Chem.* **2021**, *93*, 6323.
44. Hale, O. J.; Illes-Toth, E.; Mize, T. H.; Cooper, H. J. *Anal. Chem.* **2020**, *92*, 6811.
45. Pathak, P.; Shvartsburg, A. A. *Anal. Chem*. **2020**, *92*, 13855.
46. Pathak, P.; Shvartsburg, A. A. *Anal. Chem*. **2022**, *94*, 7041.
47. Crowe, J. E. *Annu. Rev. Immunol.* **2022**, *40*, 349.
48. Bain, B.; Brazil, M. *Nat. Rev. Drug Discov*. **2003**, *2*, 693.
49. Kűkrer, B.; Filipe, V.; van Duijn, E.; Kasper, P. T.; Vreeken, R. J.; Heck, A. J. R.; Jiskoot, W. *Pharm. Res.* **2010**, *27*, 2197.
50. Strasser, J.; de Jong, R. N.; Beurskens, F. J.; Wang, G.; Heck, A. J. R.; Schuurman, J.; Parren, P. W. H. I.; Hinterdorfer, P.; Preiner, J. *Nano Lett*. **2019**, *19*, 4787.
51. Kumar, N.; Arthur C. P.; Ciferri, C.; Matsumoto, M. L. *Science* **2020**, *367*, 1008.
52. Li, Y.; Wang, G.; Li, N.; Wang, Y.; Zhu, Q.; Chu, H.; Wu, W.; Tan, Y.; Yu, F.; Su, X. D.; Gao, N.; Xiao, J. *Science* **2020**, *367*, 1014.
53. Chouquet, A.; Pinto, A. J.; Hennicke, J.; Ling, W. L.; Bally, I.; Schwaigerlehner, L.; Thielens, N. M.; Kunert, R.; Reiser, J. P. *Front. Bioeng. Biotechnol*. **2022**, *10*, 816275.
54. Wörner, T. P.; Snijder, J.; Bennett, A.; Agbandje-McKenna, M.; Makarov, A. A.; Heck, A. J. R. *Nat. Methods* **2020**, *17*, 395.
55. Haberger, M.; Leiss, M.; Heidenreich, A. K.; Pester, O.; Hafenmair, G.; Hook, M.; Bonnington, L.; Wegele, H.; Haindl, M.; Reusch, D.; Bulau, P. *MAbs* **2016**, *8*, 331.
56. Giles, K.; Pringle, S. D.; Worthington, K. R.; Little, D.; Wildgoose, J. L.; Bateman, R. H. *Rapid Commun. Mass Spectrom.* **2004**, *18*, 2401.
57. Young, L. M.; Saunders, J. C.; Mahood, R. A.; Revill, C. H.; Foster, R. J.; Ashcroft, A. E.; Radford, S. E *Methods* **2016**, *95*, 62.
58. Pang, X.; Jia, C.; Chen, Z.; Li, L. *J. Am. Soc. Mass Spectrom.* **2017**, *28*, 110.
59. Österlund, N.; Moons, R.; Ilag, L. L.; Sobott, F.; Gräslund, A. *J. Am. Chem. Soc.* **2019**, *141*, 10440.
60. Depland, A. D.; Stroganova, I.; Wootton, C. A; Rijs, A. M. *J. Am. Soc. Mass Spectrom.* **2023**, *34*, 193.
61. Melani, R. D.; Srzentic, K.; Gerbasi, V. R.; McGee, J. P.; Huguet, R.; Fornelli, L.; Kelleher, N. L. *MAbs* **2019**, *11*, 1351.
62. Shvartsburg, A. A.; Tang, K.; Smith, R. D. *J. Am. Soc. Mass Spectrom*. **2005**, *16*, 1447.
63. Krylov, E. V.; Nazarov, E. G.; Miller, R. A *Int. J. Mass Spectrom.* **2007**, *266*, 76.
64. Konermann, L. *J. Am. Soc. Mass Spectrom.* **2017**, *28*, 1827.
65. Shvartsburg, A. A.; Li, F.; Tang, K.; Smith, R. D. *Anal. Chem*. **2006**, *78*, 3304.
66. Ieritano, C.; Featherstone, J.; Haack, A.; Guna, M.; Campbell, J. L.; Hopkins, W. S. *J. Am. Soc. Mass Spectrom.* **2020**, *31*, 582.
67. Shvartsburg, A. A.; Tang, K. Smith, R. D. *J. Am. Soc. Mass Spectrom.* **2005**, *16*, 2.

ToC graphics